# Direct Imaging of the First-Order Spin-Flop Transition in the Layered Manganite $La_{1.4}Sr_{1.6}Mn_2O_7$

U. Welp, A. Berger, D. J. Miller, V. K. Vlasko-Vlasov, K. E. Gray, and J. F. Mitchell
*Materials Science Division, Argonne National Laboratory, Argonne, Illinois 60439*
(Received 2 April 1999)

Magnetic field induced transitions in antiferromagnetic $La_{1.4}Sr_{1.6}Mn_2O_7$ were studied using magnetization measurements and a high-resolution magneto-optical imaging technique. We report the direct observation of the formation of ferromagnetic domains appearing at the first-order spin-flop transition. The magnetization proceeds through nucleation of polarized domains at crystal defect sites and not by domain wall motion. A small magnetic hysteresis is caused by the nucleation and annihilation of domains in the mixed state. The results establish a direct link between the magnetic structure on the atomic scale and the macroscopic transport and magnetic properties of the sample.

PACS numbers: 75.30.Kz, 75.50.Ee, 75.60.–d

The naturally layered manganites of composition $La_{2-2x}Sr_{1+2x}Mn_2O_7$ have attracted much recent interest since, in addition to the phenomenon of colossal magnetoresistance (CMR) [1], they exhibit a variety of coupled magnetic, electronic, and structural ground states. Depending on the doping level $x$, the interplay of superexchange and double exchange interactions between the Mn moments gives rise to competing antiferromagnetic and ferromagnetic spin arrangements [2]. For intermediate doping levels $0.5 > x > 0.32$, $La_{2-2x}Sr_{1+2x}Mn_2O_7$ is a planar ferromagnet with Curie temperatures $T_c$ of about 100 K. Concurrent with the magnetic order the $MnO_2$ bilayers become metallic, being separated from each other by insulating $(La, Sr)_2O_2$ block layers. The coupling of the magnetic and electronic transitions has been attributed to the double-exchange mechanism and deformations of the $MnO_6$ octahedra [1,3]. Recent magnetization [4] and neutron scattering [5] experiments on the $x = 0.30$ compound, $La_{1.4}Sr_{1.6}Mn_2O_7$, have shown that for this doping level the material is a type A antiferromagnet in which the ferromagnetic $MnO_2$ bilayers are stacked antiferromagnetically along the $c$ axis with the Mn moments oriented along the $c$ axis. The unique feature of this material is the occurrence of a very large, anisotropic magnetoresistance at temperatures well below the magnetic ordering temperature [3,6] and the spontaneous formation of ferromagnetic bubble domains [7].

Here we present a study of the magnetization process using magnetization measurements and magneto-optical imaging. Magneto-optical imaging allows for the direct observation of the formation of magnetic domains and provides details of the local magnetization process which are unattainable from bulk magnetization and/or conductivity measurements. At low temperatures a first-order spin-flop (metamagnetic) transition between the antiferromagnetic and polarized states is observed at a field of about 1.1 kOe applied along the $c$ axis. For intermediate field values, we find direct evidence for a mixed state of coexisting spin-flop and antiferromagnetic domains as predicted in Ref. [6]. The magnetization process in the mixed state proceeds through nucleation of spin-flop domains at crystal defect sites. Domain wall motion appears to be of minor significance, especially in the onset region of the transition. A small magnetic hysteresis, consistent with the first-order nature of the transition, is caused by the difference between the domain nucleation and annihilation processes.

Single crystals of $La_{1.4}Sr_{1.6}Mn_2O_7$ were melt grown in flowing 20% $O_2$ (balance Ar) in a floating-zone optical image furnace. The sample for the measurements described here was cleaved from the resulting polycrystalline boules [8]. It is shaped like an irregular plate (see Fig. 2 below) with lateral dimension of roughly $600 \times 800\ \mu m^2$ and thickness (along $c$) of 230 $\mu$m. The magneto-optical images were obtained using a high-resolution magneto-optical imaging technique [9]. It utilizes Faraday rotation in a Bi-doped yttrium-iron-garnet film placed on top of the sample to create a map of the magnetic induction component normal to the imaged sample surface and allows one to extend the optical study [10] of magnetic domains to nontransparent materials.

The magnetic characterization of our sample is summarized in Fig. 1. Figure 1a shows the temperature dependence of the magnetization measured in a field of 500 Oe applied along the tetragonal $c$ axis and perpendicular to this axis. The pronounced anisotropy appearing at temperatures below 70 K, with the $c$-axis magnetization dropping almost to zero, is the typical behavior of a uniaxial antiferromagnet with the magnetic moments aligned parallel to $c$. The peak in the $c$-axis data defines a Néel temperature of $T_N = 72$ K. The enhanced in-plane magnetization in the paramagnetic state has been observed previously [11] and is caused by ferromagnetic intergrowth phases commonly found in this layered material. For our measurements we chose a fairly high field of 500 Oe so as to minimize this contribution.

The field dependence of the $c$-axis magnetization at 20 K is shown in Fig. 1b for increasing ($M_{\text{in}}$) and decreasing

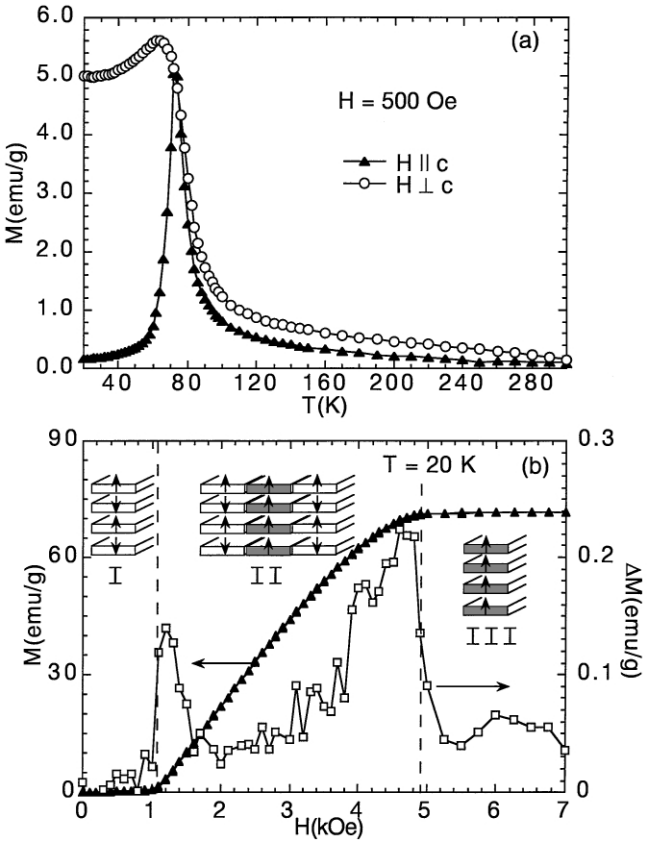


FIG. 1. (a) Temperature dependence of the magnetization measured in a field of 500 Oe applied parallel and perpendicular to the $c$ axis. (b) Field dependence of the $c$-axis magnetization at 20 K in increasing and decreasing field (left scale) and magnetization hysteresis $\Delta M$ (right scale) at 20 K. Also shown are schematics of the spin arrangements in the antiferromagnetic ("I"), mixed ("II"), and polarized ("III") phases.

($M_{\mathrm{de}}$) field. The magnetization stays essentially zero (region I) until a critical field of $H_{SF} = 1.1$ kOe is reached at which a steep, initially linear rise of the magnetization occurs. The magnetization saturates near $H_S^{\parallel} = 4.8$ kOe at a value of 72 emu/g. This magnetization behavior is indicative of a first-order spin-flop transition at $H_{SF}$. In the field region of 1.1–4.8 kOe (region II) a mixed state of coexisting antiferromagnetic and polarized domains is expected due to demagnetization effects [12]. Also shown is the magnetization hysteresis $\Delta M = M_{\mathrm{de}} - M_{\mathrm{in}}$. The magnetization process is essentially reversible; however, clearly resolved peaks of $\Delta M$ are observed near $H_{SF}$ and at $H_S^{\parallel}$. As discussed in more detail below these are caused by the nucleation of polarized and antiferromagnetic domains, respectively.

Figure 2 shows magneto-optical images of the normal component of the magnetic induction $B_z$ at the sample surface. Bright contrast in these images corresponds to high local values of $B_z$. Frames (a)–(e) correspond to the magnetization curves in Fig. 1b. At applied fields below $H_{SF}$ (Fig. 2a) the sample is in the antiferromagnetic state

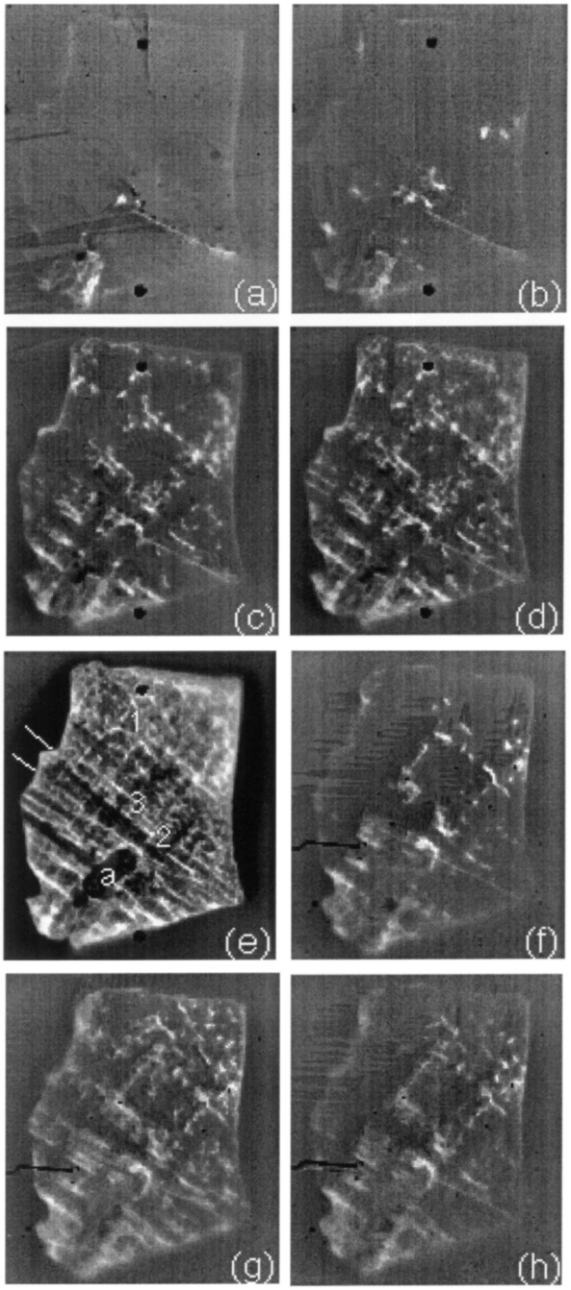


FIG. 2. Magneto-optical images of the local magnetic induction $B_z$ at the crystal surface taken at 20 K. Images (a) to (e) are taken in 1008 Oe (a), 1092 Oe (b), 1260 Oe (c), 1344 Oe (d), and 1680 Oe (e). In image (e), label "a" indicates a $(La, Sr)_2MnO_4$ inclusion; "1," "2," and "3" indicate the positions of local induction curves (see Fig. 4). The white lines mark a change in direction of the striations coinciding with a small angle grain boundary. Images (f) to (h) are taken at 1176 Oe (f), 1344 Oe (g), and 1176 Oe (h) after the sample surface has been polished by 20 $\mu$m. A comparison of (f) and (h) reveals the hysteresis between nucleation and annihilation of polarized domains. The $(La, Sr)_2MnO_4$ inclusion is visible in the lower left corner.

and correspondingly there is no magnetic contrast in the bulk of the crystal. Magnetic contrast exists only along the edges of the sample due to demagnetization effects, along a needle shaped domain extending to the lower

right corner, and near the lower left corner. The contrast near the lower left is associated with a paramagnetic $(La, Sr)_2MnO_4$ inclusion (labeled "a" in Fig. 2e), a common second phase in the $La_{2-2x}Sr_{1+2x}Mn_2O_7$ manganites [8]. With increasing field, polarized domains seen as bright spots nucleate. These images show directly the coexistence of polarized and antiferromagnetic domains as expected for the mixed state of the first-order spin-flop transition.

The magnetization process proceeds through the nucleation of new domains. The expansion of polarized domains through continuous domain wall motion as seen, for example, in the uniaxial antiferromagnets $MnF_2$ [13] and $FeCl_2$ [14] near the spin flop is not observed. This behavior may have the following reasons. The thickness, $\delta$, of domain walls in traditional ferromagnets can be estimated from $\delta \sim \pi a(J_1/2K)^{1/2}$, where $J_1$ is the exchange energy, $K$ is the anisotropy energy, and $a$ is the lattice constant. Using the available literature data for the in-plane exchange energy, $J_1 \sim 3.6 \times 10^8$ erg/cm$^3$ [15], and $K \sim 2 \times 10^6$ erg/cm$^3$ [6], we estimate a domain wall thickness of about 30 lattice constants. Such a small value implies that these domain walls can be pinned very effectively by imperfections in the underlying crystal structure which prohibits the occurrence of domain wall motion.

The smallest domains that are resolved have a diameter of about 5 $\mu$m [16]. At sufficiently high density, domains coalesce to form extended domain structures (see Figs. 2d and 2e) which exhibit clear striation along two orthogonal directions. Similar behavior has been observed on several crystals. These striations coincide with the crystallographic (100) and (010) directions. Across the dark wedge shaped area highlighted by the two white lines in Fig. 2e the direction of striation changes slightly. This area coincides with a small angle grain boundary in the crystal structure. These results indicate that the nucleation sites of the polarized domains are given by the underlying crystal defect structure. Further evidence for this conclusion arises from the observation that the pattern of domains is exactly the same on successive field sweeps and that this pattern is independent of an applied in-plane field. Since the layered manganites are characterized by a complex crystal structure and a strong dependence of their magnetic state on the doping level $x$ (the $x = 0.32$ compound is a planar ferromagnet), it is possible that slight compositional variations induced during the growth process act as effective nucleation sites.

Figure 3 shows field profiles along a horizontal line through the bright spot to the left of label 2 in Fig. 2e for several applied fields. With increasing field the profiles become increasingly complex. In addition, we observe that the local field can drop below the applied value (indicated by the dashed-dotted line for an applied field of 1680 Oe) in the vicinity of polarized regions. Such a field distribution which causes the formation of stripe domains in traditional magnets suppresses the nucleation

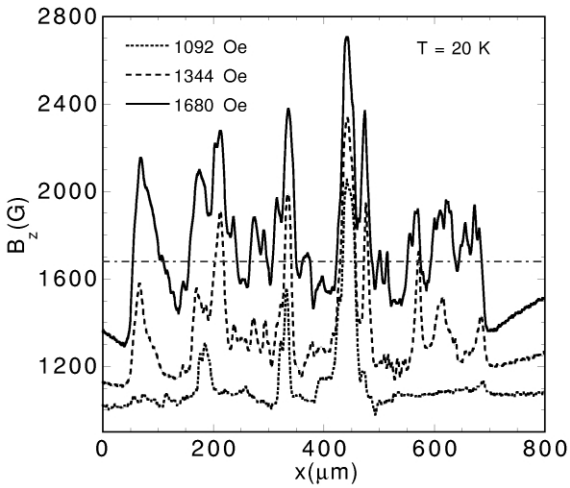


FIG. 3. Field profiles along a horizontal line through position "2" in Fig. 2e. From 1680 Oe, the applied field level is indicated by the dashed line.

of additional domains in the vicinity of existing polarized domains and thus stabilizes the striations.

Figures 2f–2h show magneto-optical images after the sample surface has been polished down by about 20 $\mu$m. The general domain pattern is not changed (compare Figs. 2d and 2g), indicating that the dominating features are not a property of a specific surface structure but a property of the bulk. However, there are changes in the arrangement of small domains upon polishing. Figures 2f and 2h show the domain pattern at 1176 Oe before and after the field has been ramped up to 1344 Oe (Fig. 2g). The observed structures are almost identical, but there is a small hysteresis between the nucleation and annihilation of polarized domains, particularly visible near the top right corner. This is the expected behavior at a first-order transition and accounts for the positive magnetization hysteresis near $H_{SF}$ shown in Fig. 1b. Similarly, the magnetization hysteresis near $H_S^{\parallel}$ is caused by the hysteresis between nucleation and annihilation of antiferromagnetic domains in a predominantly polarized material.

Figure 4 shows the field dependence of the local magnetic induction $B_z$ in selected positions on the sample surface. Here, positions 1 and 2 mark the bright spots to the left of labels 1 and 2 in Fig. 2e, and position 3 marks the dark spot to the left of 3 in Fig. 2e, respectively. For 1 and 2, discontinuous jumps of $B_z$ by about 1000 G are observed consistent with the first-order nature of the transition. Up to an external field of 1680 Oe, the highest field reached for imaging, no spin flop occurs in position 3. Instead, the local field falls below the applied field due to the stray field of the surrounding polarized regions as described above. Also included in Fig. 4 is the field dependence of $\langle B_z \rangle$, the value of the magnetic induction when averaged over the entire sample surface. This average value is determined by the global magnetization of

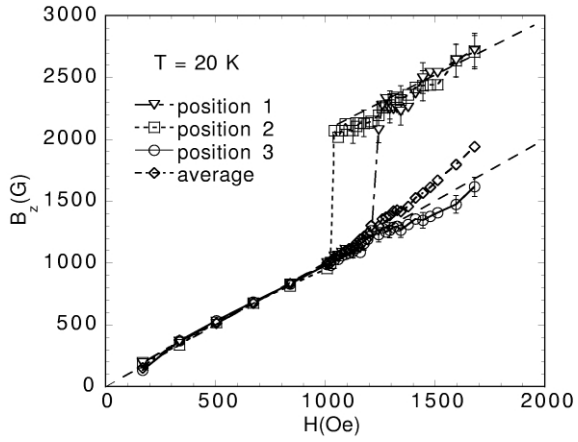


FIG. 4. Local magnetic induction curves at the positions marked in Fig. 2e. Sharp, discontinuous jumps in the induction are observed at the transition into the spin-flop phase. Also included is $\langle B_z \rangle$, the average of $B_z$ over the sample surface.

the sample (see Fig. 1b). In an applied field of 1680 G, $\langle B_z \rangle$ is about 1910 G. By solving the magnetostatic surface integrals [17] for a rectangular box with dimensions corresponding to our sample geometry, this value can be converted into a magnetization of 12 emu/g which is in good agreement with the magnetometer measurement of 14 emu/g (Fig. 1b). Similarly, the jump height of 1000 G can be converted into a saturation magnetization of 53 emu/g which is about 25% smaller than expected. This reduced value might be caused by a small gap between the sample surface and the magneto-optical film, typically several $\mu$m. This will lead to a reduction of the measured value for $B_z$ above a domain by an error that increases as the lateral size of the domain decreases. In addition a small, but finite, closure angle between the Mn moments in the spin-flop phase [6] would cause a further increase of $M$ in high fields that is not accounted for in the jump height.

The results shown in Fig. 2 can be directly related to measurements of the anisotropic magnetoconductivity of $La_{1.4}Sr_{1.6}Mn_2O_7$ [6]. The double exchange mechanism causes the intimate coupling of the electronic and magnetic state of this material. In particular, a high $c$-axis conductivity is correlated with a ferromagnetic spin alignment along the $c$ axis. Thus, the images shown in Fig. 2 can be seen as maps of the $c$-axis conductivity. Correspondingly, the sharp local steps of the induction (Fig. 4) imply extremely sharp steps in the conductivity which offers the potential for a field controlled resistive switch. The in-plane transport occurs along a parallel circuit of ferromagnetic, highly conducting $MnO_2$ bilayers in the antiferromagnetic and the fully polarized state. At the spin-flop transition, however, domain walls start appearing and cause a local reduction in $\sigma_{ab}$. As suggested in Ref. [6] this mechanism gives a direct account of the minimum of $\sigma_{ab}$ observed near $H_{SF}$.

In conclusion, magnetic transitions in the antiferromagnetic state of $La_{1.4}Sr_{1.6}Mn_2O_7$ were studied using a high-resolution magneto-optical imaging technique. We report the first direct observation of the formation of ferromagnetic domains appearing at the first-order spin-flop transition. The magnetization process proceeds through nucleation of polarized domains at crystal defect sites; domain wall motion appears to be of minor significance, especially in the onset region of the transition. A small magnetic hysteresis is caused by the nucleation and annihilation of domains in the mixed state. These results establish a direct link between the magnetic structure on the atomic scale as seen in neutron scattering and the macroscopic properties of the sample as seen in magnetization and conductivity measurements.

This work was supported by the U.S. DOE, BES Materials Sciences under Contract No. W-31-109-ENG-38. We thank Qing'An Li and R. Osborn for helpful discussions.

[1] T. Kimura *et al.*, Science **274**, 1698 (1996).
[2] M. Kubota *et al.*, cond-mat/9902288.
[3] M. Imada *et al.*, Rev. Mod. Phys. **70**, 1039 (1998); A. J. Millis, Nature (London) **392**, 147 (1998); J. B. Goodenough *et al.*, *Landolt-Börnstein* (Springer, Berlin, 1970), Vol. 40, p. 126.
[4] T. Kimura *et al.*, Phys. Rev. Lett. **79**, 3720 (1997).
[5] T. G. Perring *et al.*, Phys. Rev. B **58**, 14 693 (1998); D. N. Argyriou *et al.*, Phys. Rev. B **59**, 8695 (1999).
[6] Qing'An Li *et al.*, cond-mat/9903452.
[7] T. Fukumura *et al.*, Science **284**, 196 (1999).
[8] J. F. Mitchell *et al.*, Phys. Rev. B **55**, 63 (1997).
[9] L. A. Dorosinskii *et al.*, Physica (Amsterdam) **203C**, 149 (1992); for a recent review, see, V. K. Vlasko-Vlasov *et al.*, in *Physics and Materials Science of Vortex States, Flux Pinning and Dynamics*, edited by R. Kossowsky *et al.* (Kluwer Academic, Dordrecht, The Netherlands, 1999), p. 205.
[10] J. F. Dillon, J. Magn. Magn. Mater. **84**, 213 (1990); A. K. Zvezdin, in *Handbook of Magnetic Materials*, edited by K. H. J. Buschow (Elsevier, Amsterdam, 1995), Vol. 9, p. 405, and references therein.
[11] S. D. Bader *et al.*, J. Appl. Phys. **83**, 6385 (1998); C. D. Potter *et al.*, Phys. Rev. B **57**, 72 (1998).
[12] B. E. Keen *et al.*, J. Appl. Phys. **37**, 1120 (1966); I. S. Jacob and P. E. Lawrence Phys. Rev. **164**, 866 (1967); V. G. Baryakhtar *et al.*, Sov. Phys. Solid State **26**, 231 (1984).
[13] A. R. King and D. Paquette, Phys. Rev. Lett. **30**, 662 (1973).
[14] J. F. Dillon *et al.*, Solid State Commun. **16**, 371 (1975).
[15] S. Rosenkranz *et al.* (to be published); H. Fujioka *et al.*, cond-mat/9902253. These experiments were performed on the $x = 0.4$ material which we consider a good estimate for the $x = 0.3$ compound.
[16] The resolution that can typically be achieved is $2-3$ $\mu$m.
[17] J. D. Jackson *Classical Electrodynamics*, (Wiley, New York, 1975), Chap. 5.